nature medicine

Abnormal development of NG2$^+$PDGFR-α^+ neural progenitor cells leads to neonatal hydrocephalus in a ciliopathy mouse model

Calvin S Carter[1,10], Timothy W Vogel[2,10], Qihong Zhang[3,4], Seongjin Seo[4,5], Ruth E Swiderski[3,4], Thomas O Moninger[6], Martin D Cassell[7], Daniel R Thedens[8], Kim M Keppler-Noreuil[3], Peggy Nopoulos[9], Darryl Y Nishimura[3], Charles C Searby[3,4], Kevin Bugge[3,4] & Val C Sheffield[3,4]

Hydrocephalus is a common neurological disorder that leads to expansion of the cerebral ventricles and is associated with a high rate of morbidity and mortality. Most neonatal cases are of unknown etiology and are likely to have complex inheritance involving multiple genes and environmental factors. Identifying molecular mechanisms for neonatal hydrocephalus and developing noninvasive treatment modalities are high priorities. Here we use a hydrocephalic mouse model of the human ciliopathy Bardet-Biedl Syndrome (BBS) and identify a role for neural progenitors in the pathogenesis of neonatal hydrocephalus. We found that hydrocephalus in this mouse model is caused by aberrant platelet-derived growth factor receptor α (PDGFR-α) signaling, resulting in increased apoptosis and impaired proliferation of chondroitin sulfate proteoglycan 4 (also known as neuron-glial antigen 2 or NG2)$^+$PDGFR-α^+ neural progenitors. Targeting this pathway with lithium treatment rescued NG2$^+$PDGFR-α^+ progenitor cell proliferation in BBS mutant mice, reducing their ventricular volume. Our findings demonstrate that neural progenitors are crucial in the pathogenesis of neonatal hydrocephalus, and we identify new therapeutic targets for this common neurological disorder.

Neonatal hydrocephalus is a common disorder affecting the human nervous system with an estimated incidence of 1–3 per 1,000 live births[1–4], creating a healthcare burden of $2 billion annually[5,6]. Hydrocephalus leads to the expansion of cerebral ventricles and is frequently associated with morbidity and mortality[7–9]. This disease remains understudied despite being a common developmental anomaly[10]. There are multiple causes of hydrocephalus, including obstruction of cerebrospinal fluid (CSF) flow and CSF overproduction; however, a substantial portion of this disease is idiopathic in nature[9–16]. Current therapies rely on invasive procedures that are associated with high failure and complication rates, making the identification of molecular mechanisms underlying neonatal hydrocephalus a high priority for the medical community[3,9,11,17,18].

Recently, mouse models with impaired cilia function have provided insight into the mechanisms involved in hydrocephalus occurring in the absence of obstruction, a condition known as communicating hydrocephalus[10,13,14,19,20]. Mutations in genes that disrupt ependymal motile cilia structure and function hinder the beat frequency of ependymal motile cilia and CSF flow, leading to the development of hydrocephalus[13,14,19,20]. Nonmotile cilia known as primary cilia extend from the surface of nearly all cell types. Primary cilia serve as sensory antennae facilitating many signaling pathways, including the Wnt[21], sonic hedgehog (Shh)[22,23] and PDGFR-α[24] pathways, enabling cells to respond to developmental cues at several sites of neurogenesis in the central nervous system, including the periventricular regions[25]. These nonmotile cilia are required for the normal development of neural progenitor cells (NPCs)[26,27].

Recent findings have demonstrated that ependymal motile cilia and CSF flow are required for the normal development of NPCs, suggesting an intimate link between the ventricular system and neural development[28]. The close proximity of NPCs to the periventricular regions suggests that these cells have a role in maintaining the integrity of the ventricular system[25,29]. However, a role for NPCs in the pathophysiology of hydrocephalus has not been studied. In this study we investigated whether abnormal signaling through primary cilia in NPCs may contribute to the genesis of neonatal hydrocephalus. To test this hypothesis, we used a mouse model of a genetically heterogeneous autosomal recessive human disorder with impaired cilia known as BBS that is caused by mutations in 17 genes, 7 of which (*BBS1*, *BBS2*, *BBS4*, *BBS5*, *BBS7*, *BBS8* and *BBS9*) form a complex known as the BBSome[30]. The cardinal features of BBS include retinal degeneration, obesity and cognitive delay[19]. Some patients with BBS

[1]Graduate Program in Neuroscience, University of Iowa Carver College of Medicine, Iowa City, Iowa, USA. [2]Department of Neurosurgery, University of Iowa Carver College of Medicine, Iowa City, Iowa, USA. [3]Department of Pediatrics, Division of Medical Genetics, University of Iowa Carver College of Medicine, Iowa City, Iowa, USA. [4]Howard Hughes Medical Institute, University of Iowa Carver College of Medicine, Iowa City, Iowa, USA. [5]Department of Ophthalmology, University of Iowa Carver College of Medicine, Iowa City, Iowa, USA. [6]Central Microscopy Research Facilities, University of Iowa Carver College of Medicine, Iowa City, Iowa, USA. [7]Department of Anatomy and Cell Biology, University of Iowa Carver College of Medicine, Iowa City, Iowa, USA. [8]Department of Radiology, University of Iowa Carver College of Medicine, Iowa City, Iowa, USA. [9]Department of Psychiatry, University of Iowa Carver College of Medicine, Iowa City, Iowa, USA. [10]These authors contributed equally to this work. Correspondence should be addressed to V.C.S. (val-sheffield@uiowa.edu).

Received 4 June; accepted 12 October; published online 18 November 2012; doi:10.1038/nm.2996

have enlarged cerebral ventricles, and all BBS mouse models have communicating hydrocephalus[19,31,32]. Here we demonstrate that abnormal development of NPCs specifically expressing NG2 and PDGFR-α leads to the development of neonatal ventriculomegaly in BBS mice. Our findings identify a new mechanism underlying hydrocephalus and provide a therapeutic target for treatment.

RESULTS

BBS mutant mice develop neonatal hydrocephalus

We have previously shown that BBS mutant mice homozygous for the most common human BBS mutation (*Bbs1*$^{M390R/M390R}$ mice) develop ventricular dilatation similar to that reported in human patients with BBS[19,31,32] (**Fig. 1a**,**b**). Ventriculomegaly in *Bbs1*$^{M390R/M390R}$ mice is fully penetrant and accompanied by neurological deficits, similar to in patients with hydrocephalus[3,9,19,31,32]. We use the term hydrocephalus in *Bbs1*$^{M390R/M390R}$ mice to describe the ventriculomegaly that has been previously reported in other mouse models[4,9,10,14–16,20].

We first examined the time of onset of hydrocephalus in *Bbs1*$^{M390R/M390R}$ brains by examining H&E-stained sections. Dilation of the lateral ventricles began between postnatal day (P) 0 and P3 in *Bbs1*$^{M390R/M390R}$ mice (**Fig. 1c**,**d**). Notably, this timing is before the maturation of ependymal motile cilia, which occurs from P5–P10 (refs. 10,13,14), suggesting that the onset of hydrocephalus in *Bbs1*$^{M390R/M390R}$ mice occurs independently of ependymal motile cilia function (**Fig. 1e**).

Aberrant apoptosis and proliferation in *Bbs1* mice

We next studied whether known causes of hydrocephalus contribute to the phenotype in *Bbs1*$^{M390R/M390R}$ mice. Injection of Evans blue dye showed no evidence of obstructive hydrocephalus (**Supplementary Fig. 1**). We found no evidence of excess CSF production in *Bbs1*$^{M390R/M390R}$ mice on the basis of normal choroid plexus ultrastructure and CSF ion concentrations (**Supplementary Fig. 1**).

We therefore sought to identify other potential mechanisms that may contribute to the early development of communicating hydrocephalus in *Bbs1*$^{M390R/M390R}$ mice. Previous work has shown that these mice have a small corpus striatum[19]. Moreover, patients with BBS have reduced white and gray matter volume in the periventricular regions[31,32]. Therefore, we examined apoptosis and cell proliferation in the periventricular regions in *Bbs1*$^{M390R/M390R}$ mice to determine whether cell loss contributes to the pathophysiology of neonatal hydrocephalus. Immunofluorescent analysis using TUNEL, a marker of apoptotic cells, and BrdU, a marker of proliferating cells, identified TUNEL$^+$ cells adjacent to the lateral ventricles and BrdU$^+$ cells in the subventricular zone (SVZ) in both wild-type (WT) and *Bbs1*$^{M390R/M390R}$ mice (**Fig. 2a**). Quantification revealed that the *Bbs1*$^{M390R/M390R}$ mice had a twofold higher rate of apoptosis and a 50% reduction in cell proliferation in the periventricular regions at P3 and P7 relative to WT mice (**Fig. 2b**).

Abnormal development of NG2$^+$PDGFR-α$^+$ cells in *Bbs1* mice

We next investigated the cell type that is responsible for the imbalance in apoptosis and cell proliferation by examining a number of markers of NPCs, neurons and glia. Using immunofluorescence, we double stained coronal brain slices from WT and *Bbs1*$^{M390R/M390R}$ neonates with either TUNEL or BrdU and markers of these major cell types. We found no significant differences between WT and *Bbs1*$^{M390R/M390R}$ brains in the number of TUNEL-labeled cells also staining positive for markers of developing (Nestin) and mature neurons (NeuN), astrocytes (glial fibrillary acidic protein (GFAP)) and oligodendrocytes[33–35] (O4; **Fig. 3a** and **Supplementary Fig. 2**). Notably, we found that nearly all TUNEL$^+$ cells in both WT and *Bbs1*$^{M390R/M390R}$ mice expressed NG2 and PDGFR-α, two markers of oligodendrocyte precursor cells (OLPs)[36–40]. Quantification revealed that a larger proportion (greater than twofold) of the TUNEL-labeled cells were also NG2$^+$ and PDGFR-α$^+$ in *Bbs1*$^{M390R/M390R}$ mice compared to in WT mice (**Fig. 3a**). NG2 and PDGFR-α have previously been shown to mark a particular class of OLPs that are expressed early in the lineage termed NG2$^+$PDGFR-α$^+$ NPCs[36–40]. We also examined Olig2, a Shh-induced basic helix-loop-helix transcription factor that is expressed later in the oligodendrocytic lineage than

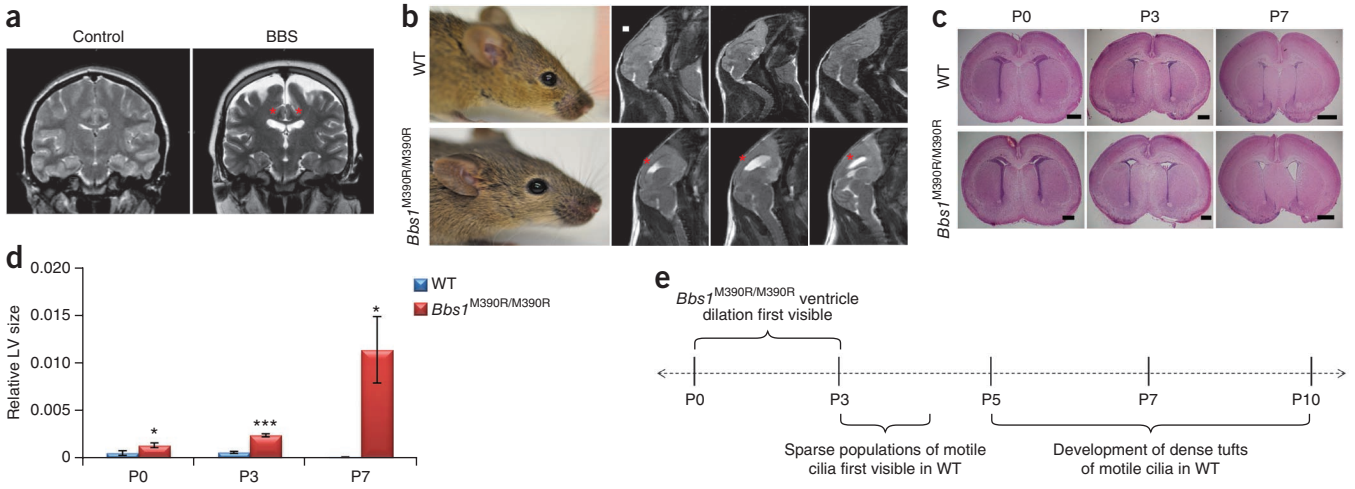

Figure 1 Hydrocephalus in BBS mutant mice occurs before motile cilia develop. (**a**) T2-weighted coronal MRI scans of a patient with BBS and an age- and sex-matched control (unaffected) individual showing ventriculomegaly of the lateral ventricles (red asterisks). (**b**) Images of 3-month-old WT and *Bbs1*$^{M390R/M390R}$ mice showing a normal cranial vault in both (left). T2-weighted sagittal MRI scans showing hydrocephalus of the lateral ventricles (red asterisks) in the *Bbs1*$^{M390R/M390R}$ mouse (right). Scale bar, 1 mm. (**c**,**d**) Histology of WT and *Bbs1*$^{M390R/M390R}$ neonates showing perinatal onset of hydrocephalus in mutant pups (**c**) and quantifications (**d**) showing ventricular dilation beginning at P0. LV, lateral ventricle. All data are shown as the means ± s.e.m. $^*P < 0.05$, $^{***}P < 0.0005$ determined by unpaired *t* test. Scale bars, P0 and P3, 500 μm; P7, 1 mm. (**e**) Timeline of the genesis of hydrocephalus in BBS mutant mice relative to motile cilia development showing that *Bbs1*$^{M390R/M390R}$ mice develop hydrocephalus before motile cilia[13,14]. All experiments used at least three mice per group and genotype.

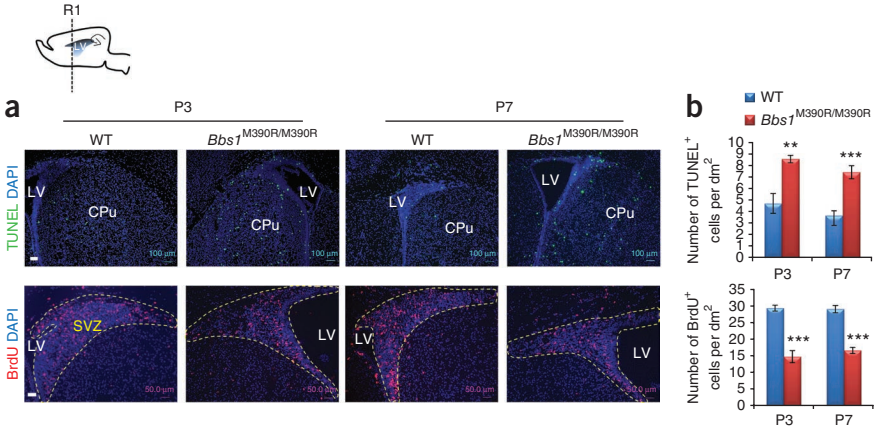

Figure 2 Increased apoptosis and reduced proliferation in the brains of *Bbs1*$^{M390R/M390R}$ mice. On the top left is a cartoon depiction of the sagittal section of a mouse brain showing the region of subsequent analyses (R1). LV, lateral ventricle. (**a**,**b**) Representative immunofluorescent images (**a**) and quantification (**b**) of cells labeled with TUNEL (top) or BrdU (bottom) per area in WT and *Bbs1*$^{M390R/M390R}$ brains at P3 and P7. All experiments used at least three mice per group and genotype (dashed yellow lines outline the SVZ). All data are shown as the means ± s.e.m. $^{**}P < 0.005$, $^{***}P < 0.0005$ determined by unpaired *t* test. Scale bars, 100 μm (**a**, top) and 50 μm (**a**, bottom). CPu, caudate putamen.

NG2 and PDGFR-α, which are both rapidly downregulated when differentiation to oligodendrocytes occurs[36–39]. We found no significant overlap between TUNEL$^+$ and Olig2$^+$ cells, indicating that in both WT and *Bbs1*$^{M390R/M390R}$ mice, mature OLPs and oligodendrocytes are not undergoing apoptosis (**Fig. 3a**). Quantification revealed no significant difference between WT and *Bbs1*$^{M390R/M390R}$ mice in the number of TUNEL$^+$ cells also labeled with Olig2 ($P = 0.29$; **Fig. 3a**).

We then investigated the identity of the proliferating cells. We found that NG2$^+$, PDGFR-α$^+$ and Olig2$^+$ OLPs comprised a large portion of the BrdU$^+$ cells in the SVZ of WT mice (**Fig. 3b**). However, in *Bbs1*$^{M390R/M390R}$ brains, there were approximately 50% fewer BrdU-labeled NG2$^+$PDGFR-α$^+$ cells in the SVZ (**Fig. 3b**). WT and BBS mutant mice did not differ in the number of Olig2$^+$ cells undergoing cell proliferation (BrdU$^+$) ($P = 0.39$; **Fig. 3b**). There was also no significant difference between WT and *Bbs1*$^{M390R/M390R}$ mice with respect to the other cell markers examined (**Fig. 3b** and **Supplementary Fig. 2**).

We then quantified the number of NG2$^+$, PDGFR-α$^+$ and Olig2$^+$ cells within the SVZ to determine the effect of impaired survival and proliferation in these precursor cells. We found significantly ($P < 0.05$) fewer of these cell populations in the SVZ of *Bbs1*$^{M390R/M390R}$ brains relative to the SVZ of WT brains (**Supplementary Fig. 3**).These results demonstrate that NG2$^+$PDGFR-α$^+$ NPCs have increased apoptosis and reduced proliferation, leading to reduced OLP populations in the brains of *Bbs1*$^{M390R/M390R}$ mice.

Conditional knockout of *Bbs1* leads to neonatal hydrocephalus

To confirm the involvement of NG2$^+$PDGFR-α$^+$ NPCs in the genesis of neonatal hydrocephalus in BBS, we generated conditional knockout

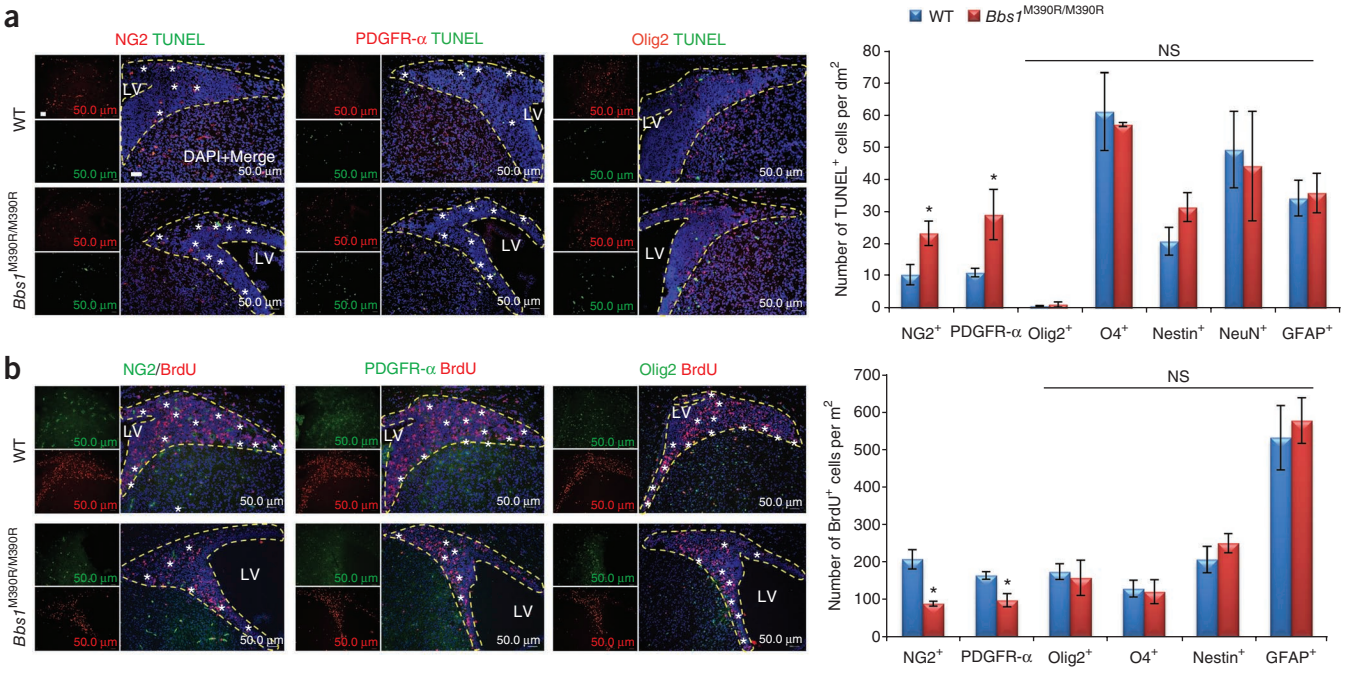

Figure 3 Impaired survival and proliferation of NG2$^+$PDGFR-α$^+$ neural progenitor cells in *Bbs1*$^{M390R/M390R}$ mice. (**a**,**b**) Representative immunofluorescent images showing TUNEL-labeled (**a**) and BrdU-labeled (**b**) cells also expressing NG2, PDGFR-α or Olig2. Quantifications are also shown (**a**,**b**, right). At least three mice per group and genotype were analyzed. All dashed yellow lines outline the SVZ. White asterisks highlight cells with overlap of TUNEL or BrdU and a cell type marker. All data shown are the means ± s.e.m. $^{*}P < 0.05$, NS, not significant determined by unpaired *t* test. Scale bars, 50 μm. CPu, caudate putamen; LV, lateral ventricle.

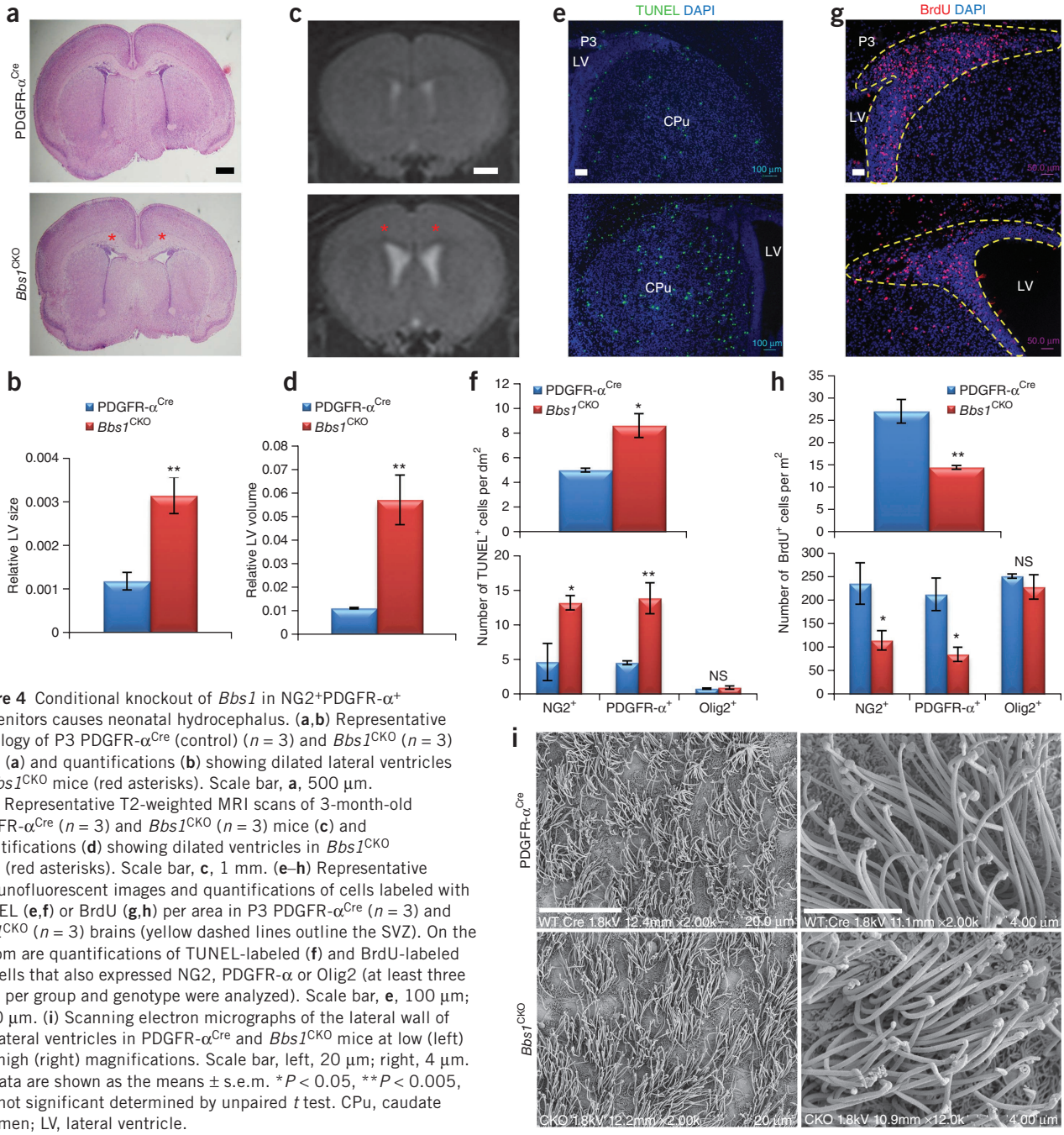

Figure 4 Conditional knockout of *Bbs1* in NG2⁺PDGFR-α⁺ progenitors causes neonatal hydrocephalus. (**a**,**b**) Representative histology of P3 PDGFR-α^{Cre} (control) ($n = 3$) and *Bbs1*^{CKO} ($n = 3$) pups (**a**) and quantifications (**b**) showing dilated lateral ventricles of *Bbs1*^{CKO} mice (red asterisks). Scale bar, **a**, 500 μm. (**c**,**d**) Representative T2-weighted MRI scans of 3-month-old PDGFR-α^{Cre} ($n = 3$) and *Bbs1*^{CKO} ($n = 3$) mice (**c**) and quantifications (**d**) showing dilated ventricles in *Bbs1*^{CKO} mice (red asterisks). Scale bar, **c**, 1 mm. (**e**–**h**) Representative immunofluorescent images and quantifications of cells labeled with TUNEL (**e**,**f**) or BrdU (**g**,**h**) per area in P3 PDGFR-α^{Cre} ($n = 3$) and *Bbs1*^{CKO} ($n = 3$) brains (yellow dashed lines outline the SVZ). On the bottom are quantifications of TUNEL-labeled (**f**) and BrdU-labeled (**h**) cells that also expressed NG2, PDGFR-α or Olig2 (at least three mice per group and genotype were analyzed). Scale bar, **e**, 100 μm; **g**, 50 μm. (**i**) Scanning electron micrographs of the lateral wall of the lateral ventricles in PDGFR-α^{Cre} and *Bbs1*^{CKO} mice at low (left) and high (right) magnifications. Scale bar, left, 20 μm; right, 4 μm. All data are shown as the means ± s.e.m. $^*P < 0.05$, $^{**}P < 0.005$, NS, not significant determined by unpaired *t* test. CPu, caudate putamen; LV, lateral ventricle.

mice lacking *Bbs1* in PDGFR-α–expressing NPCs (*Bbs1*$^{loxP/loxP}$ × *Pdgfra*^{Cre}, termed here *Bbs1*^{CKO} mice). *Bbs1* mRNA was almost completely absent in the cortex and its levels were significantly ($P < 0.05$) reduced in the hypothalamus of *Bbs1*^{CKO} mice; moreover, Cre was expressed in NG2⁺, PDGFR-α⁺ and Olig2⁺ NPCs but not in the ependymal cells lining the ventricles (**Supplementary Fig. 4a**,**b**). These findings indicate that *Bbs1* knockout in *Bbs1*^{CKO} mice is specific to a particular class of periventricular NPCs in the cortex and hypothalamus. *Bbs1*^{CKO} mice have hydrocephalus with an onset at P3 in the absence of obstruction (**Fig. 4a**–**d** and **Supplementary Fig. 4c**,**d**). Moreover, neonatal hydrocephalus in *Bbs1*^{CKO} mice was 100% penetrant. TUNEL and BrdU staining revealed a twofold increase in the number of apoptotic cells (**Fig. 4e**,**f**) and a 50% reduction in the number of proliferating cells in *Bbs1*^{CKO} mice relative to in PDGFR-α^{Cre} mice (controls) (**Fig. 4g**,**h**). We found that nearly all TUNEL⁺ cells and a majority of BrdU⁺ cells in the SVZ in PDGFR-α^{Cre} and *Bbs1*^{CKO} mice also stained positive for NG2, PDGFR-α and, to a lesser extent, Olig2 (**Supplementary Fig. 5a**,**b**). Quantification revealed an approximately twofold increase and a 50% reduction in the number of TUNEL- and BrdU-labeled NG2⁺PDGFR-α⁺ cells, respectively, in *Bbs1*^{CKO} brains relative to control brains (**Fig. 4f**,**h**). We found no significant differences in the number of Olig2-labeled cells undergoing apoptosis (TUNEL⁺, $P = 0.32$) or replication (BrdU⁺, $P = 0.22$; **Fig. 4f**,**h**). These results demonstrate that the normal development of NG2⁺PDGFR-α⁺ NPCs is disrupted after *Bbs1* knockout in this specific cell type. Moreover, these results confirm the involvement

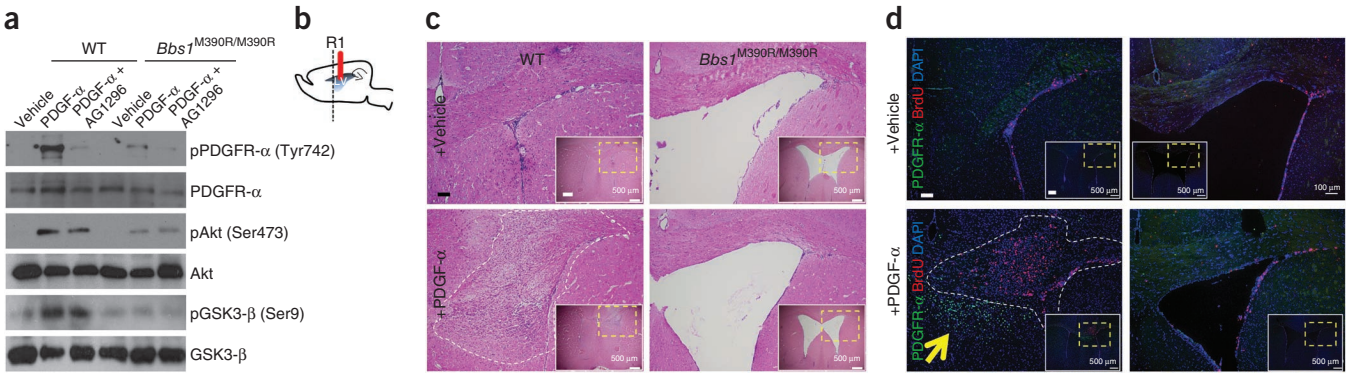

Figure 5 PDGFR-α signaling is impaired in BBS. (**a**) PDGF-α stimulation activates downstream signaling in primary oligodendrocytic precursor cells derived from WT but not *Bbs1*$^{M390R/M390R}$ brains. LV, lateral ventricle. pPDGFR-α (Tyr742), PDGFR-α phosphorylated at Tyr742; pAkt (Ser473), Akt phosphorylated at Ser 473; pGSK3-β (Ser9), GSK3-β phosphorylated at Ser9. (**b**) Cartoon depicting the sagittal section of a mouse brain showing the cannula implantation site (solid red line) and the region of subsequent analyses (R1). (**c**) Representative histology of the ipsilateral brain hemisphere of vehicle (PBS)-infused WT ($n = 7$) and *Bbs1*$^{M390R/M390R}$ ($n = 7$) mice (top) and PDGF-α–infused WT ($n = 7$) and *Bbs1*$^{M390R/M390R}$ ($n = 7$) mice (bottom). The insets show low-magnification images, with the regions of interest (enlarged in the larger images) outlined by yellow dotted lines. Scale bar, larger images, 100 μm; insets, 500 μm. (**d**) Representative immunofluorescent images of the ipsilateral infused hemisphere showing cells labeled with BrdU and PDGFR-α in vehicle-infused WT ($n = 3$) and *Bbs1*$^{M390R/M390R}$ ($n = 3$) mice and PDGF-α–infused WT ($n = 3$) and *Bbs1*$^{M390R/M390R}$ ($n = 3$) mice. The yellow arrow points to the hyperplastic nodule consisting of PDGFR-α$^+$ cells, and the white dashed line outlines the hyperplastic nodules in PDGF-α–infused WT mice. The insets show low-magnification images, with the regions of interest (enlarged in the larger images) outlined by yellow dotted lines. Scale bar, larger images, 100 μm; insets, 500 μm.

of NG2$^+$PDGFR-α$^+$ NPCs in the development of normal cerebral ventricles, disruption of which results in neonatal hydrocephalus.

We then investigated whether dysfunctional motile cilia could contribute to the dilated ventricles in *Bbs1*^{CKO} brains. We examined the ultrastructure of the motile cilia in PDGFR-α^{Cre} and *Bbs1*^{CKO} brains at P14 and 3 months of age and found no abnormalities in the ultrastructure or number of tufts of motile cilia in the lateral ventricles of the *Bbs1*^{CKO} brains (**Fig. 4i**). This finding provides further evidence that hydrocephalus in BBS is caused by motile cilia–independent processes.

Bbs1 is required for PDGFR-α signaling

We next examined cellular signaling pathways to assess the cause of the impaired survival and proliferation of NG2$^+$PDGFR-α$^+$ NPCs. We studied the PDGFR-α signaling pathway because it has a major role in the survival and proliferation of NG2$^+$PDGFR-α$^+$ NPCs[36–40]. We cultured primary OLPs from WT and *Bbs1*$^{M390R/M390R}$ neonates. Treatment of WT cultures with PDGF-α, which specifically binds to PDGFR-α, resulted in a large increase in the phosphorylation of PDGFR-α and the two downstream effector proteins AKT, a master regulator of cell survival and proliferation, and glycogen synthase kinase 3 β (GSK3-β), which regulates cell proliferation[41–43] (**Fig. 5a**). We showed the specificity of the response to PDGF-α in WT cultures using pretreatment with the PDGFR inhibitor AG1296, which reduced the response to PDGF-α. *Bbs1*$^{M390R/M390R}$-derived OLP cultures showed a blunted phosphorylation response to PDGF-α stimulation (**Fig. 5a**).

To confirm these findings *in vivo*, we infused PDGF-α into the lateral ventricles of WT and *Bbs1*$^{M390R/M390R}$ mice for 6 days. All infused WT mice developed atypical hyperplasias in either the medial or lateral wall of the ipsilateral ventricle, whereas none of the treated *Bbs1*$^{M390R/M390R}$ mice showed this response (**Fig. 5b**,**c**). Furthermore, the hyperplastic nodules in WT infused brains contained a large proportion of small, round proliferating (BrdU$^+$) cells (**Fig. 5c**,**d**). Immunostaining also identified a large increase in the population of PDGFR-α$^+$ NPCs in the medial wall of the PDGF-α–infused lateral ventricle in WT mice but not in *Bbs1*$^{M390R/M390R}$ mice (**Fig. 5d**). These findings demonstrate that *Bbs1*$^{M390R/M390R}$ NG2$^+$PDGFR-α$^+$ NPCs do not respond to PDGF-α and implicate a mechanism underlying the impaired survival and proliferation of NPCs in BBS. To study the role of BBS proteins in PDGFR-α signaling, we performed immunoprecipitation experiments. *In vitro* and *in vivo* experiments revealed that PDGFR-α physically interacts with the BBSome (**Supplementary Fig. 6a**,**b**). These findings indicate a mechanism underlying the impaired PDGFR-α signaling in BBS.

Lithium therapy rescues hydrocephalus

We modified the neonatal hydrocephalic phenotype in *Bbs1*$^{M390R/M390R}$ mice during the crucial perinatal period by targeting defective PDGFR-α signaling and OLP development. Lithium has been shown to enhance the proliferation and promote the survival of NPCs by stimulating phosphorylation of two downstream effectors in the PDGFR-α pathway, AKT and GSK3-β[44–46]. We treated *Bbs1*$^{M390R/+}$ heterozygous pregnant females, which were previously mated to heterozygous male mice, with lithium chloride or an equimolar sodium chloride solution administered in drinking water beginning at embryonic day (E) 14.5 (**Fig. 6a**). Histological analysis of P14 WT and *Bbs1*$^{M390R/M390R}$ brains revealed that lithium treatment in WT mice has no significant effect (sodium chloride compared to lithium chloride in WT mice, $P = 0.17$), whereas lithium treatment of *Bbs1*$^{M390R/M390R}$ mice ($n = 9$) resulted in an approximately 50% reduction in the cross-sectional area of the lateral ventricles relative to sodium chloride–treated *Bbs1*$^{M390R/M390R}$ mice ($n = 5$; **Fig. 6a–c**). Magnetic resonance imaging (MRI) at 3 months of age revealed that the ventricular volume of the lithium-treated WT mice did not differ from that of the sodium chloride–treated WT mice ($P = 0.16$; **Fig. 6b**,**c**). However, lithium-treated *Bbs1*$^{M390R/M390R}$ mice showed an approximately 50% reduction in ventricle volume relative to control-treated *Bbs1*$^{M390R/M390R}$ mice (**Fig. 6b**,**c**). We found these effects of lithium in all treated *Bbs1*$^{M390R/M390R}$ mice.

To study the mechanism underlying the effect of lithium on neonatal hydrocephalus, we examined cell proliferation and apoptosis in the

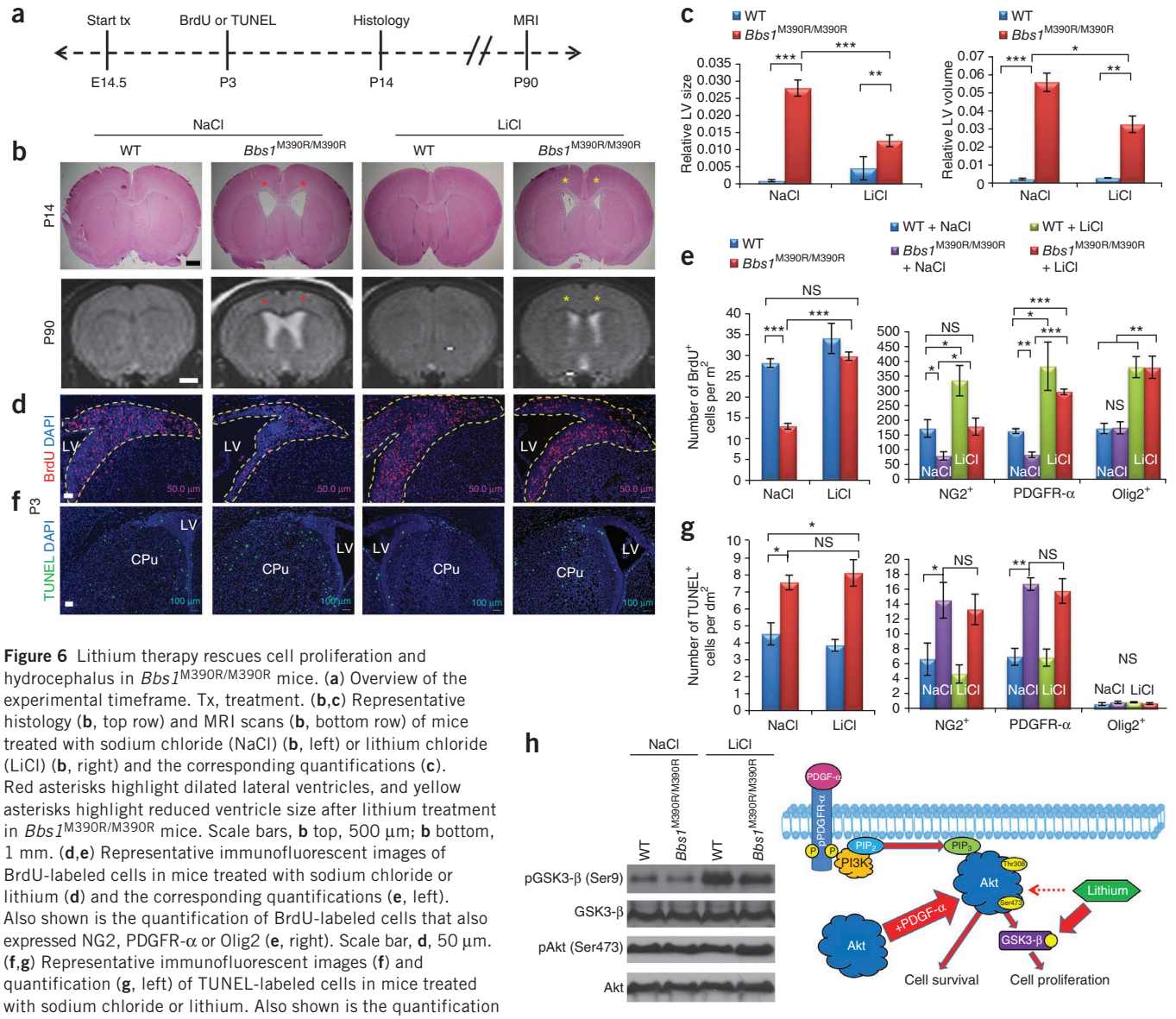

Figure 6 Lithium therapy rescues cell proliferation and hydrocephalus in *Bbs1*$^{M390R/M390R}$ mice. (**a**) Overview of the experimental timeframe. Tx, treatment. (**b**,**c**) Representative histology (**b**, top row) and MRI scans (**b**, bottom row) of mice treated with sodium chloride (NaCl) (**b**, left) or lithium chloride (LiCl) (**b**, right) and the corresponding quantifications (**c**). Red asterisks highlight dilated lateral ventricles, and yellow asterisks highlight reduced ventricle size after lithium treatment in *Bbs1*$^{M390R/M390R}$ mice. Scale bars, **b** top, 500 μm; **b** bottom, 1 mm. (**d**,**e**) Representative immunofluorescent images of BrdU-labeled cells in mice treated with sodium chloride or lithium (**d**) and the corresponding quantifications (**e**, left). Also shown is the quantification of BrdU-labeled cells that also expressed NG2, PDGFR-α or Olig2 (**e**, right). Scale bar, **d**, 50 μm. (**f**,**g**) Representative immunofluorescent images (**f**) and quantification (**g**, left) of TUNEL-labeled cells in mice treated with sodium chloride or lithium. Also shown is the quantification of TUNEL-labeled cells also expressing NG2, PDGFR-α or Olig2 (**g**, right). Scale bar, **g**, 100 μm. (**h**) Representative western blots of cortices from P3 WT and *Bbs1*$^{M390R/M390R}$ mice treated with sodium chloride or lithium (left). pGSK3-β (Ser9), GSK3-β phosphorylated at Ser9; pAkt (Ser473), Akt phosphorylated at Ser473. Drawing depicting the proposed mechanism of the effect of lithium on cell proliferation in treated WT and *Bbs1*$^{M390R/M390R}$ mice (right). Lithium increases the phosphorylation of GSK3-β, leading to an increase in cell proliferation. All data are the means ± s.e.m. $*P < 0.05$, $**P < 0.005$, $***P < 0.0005$, NS, not significant determined by unpaired *t* test. All experiments used at least three mice per group and genotype. CPu, caudate putamen; LV, lateral ventricle.

periventricular regions of P3 mice using BrdU and TUNEL assays, respectively. Staining revealed that lithium treatment had no significant effect on the number of proliferating or apoptotic cells in WT mice (sodium chloride compared to lithium chloride in WT mice: BrdU, $P = 0.29$; TUNEL, $P = 0.21$; **Fig. 6d**–**g**). However, lithium treatment resulted in an approximately twofold increase in the number of proliferating cells in *Bbs1*$^{M390R/M390R}$ mice relative to sodium chloride treatment (**Fig. 6d**,**e**). Notably, there was no significant difference in the number of proliferating cells in sodium chloride–treated WT mice and lithium-treated *Bbs1*$^{M390R/M390R}$ mice, indicating a complete rescue of the cell proliferation defect ($P = 0.16$; **Fig. 6d**,**e**). There was also no significant difference in the number of apoptotic cells in sodium chloride–treated and lithium-treated *Bbs1*$^{M390R/M390R}$ mice, indicating that the effect of lithium is specific to cell proliferation ($P = 0.29$; **Fig. 6f**,**g**). Furthermore, lithium treatment specifically rescued NG2$^+$PDGFR-α$^+$ NPC proliferation but not apoptosis in *Bbs1*$^{M390R/M390R}$ mice (sodium chloride compared to lithium chloride in *Bbs1*$^{M394R/M394R}$ mice: NG2$^+$, $P = 0.36$; PDGFR-α$^+$, $P = 0.38$) (**Fig. 6e**,**g** and **Supplementary Figs. 7** and **8**). Lithium treatment also increased the number of proliferating Olig2$^+$ cells in WT and *Bbs1*$^{M390R/M390R}$ mice by more than twofold (**Fig. 6e** and **Supplementary Fig. 7**).

To determine the molecular mechanisms underlying the effects of lithium treatment, we examined the phosphorylation of AKT and GSK3-β. Western blot analysis revealed that lithium treatment increased the phosphorylation of GSK3-β but had no effect on the phosphorylation of AKT (**Fig. 6h**). These results indicate that defective NG2$^+$PDGFR-α$^+$ NPC development leads to neonatal hydrocephalus in *Bbs1*$^{M390R/M390R}$ mice. Targeting the defective PDGFR-α

signaling pathway in these NPCs rescues the proliferation of these cells, resulting in a partial rescue of hydrocephalus.

DISCUSSION

Hydrocephalus is a complex disorder involving multiple genetic and environmental components[3,4,9]. Thus, any single pathway or mechanism will not fully explain hydrocephalus in its entirety. Previous studies have implicated impaired ependymal motile cilia, CSF overproduction and cortical atrophy in the genesis of communicating hydrocephalus[4,10,13–16,20,47]. Here we demonstrate that NG2$^+$PDGFR-α$^+$ NPCs have a key role in the pathogenesis of hydrocephalus. We found that impaired PDGFR-α signaling in *Bbs1*$^{M390R/M390R}$ mice leads to increased apoptosis and reduced proliferation of NG2$^+$PDGFR-α$^+$ NPCs, resulting in hydrocephalus. We have also demonstrated that dysfunctional motile cilia are not the primary cause of neonatal hydrocephalus in BBS mouse models, as evidenced by ventricular dilation occurring before the development of motile cilia and the fact that ependymal cilia remain intact in mice lacking *Bbs1* in PDGFR-α$^+$ cells. We have not excluded the possibility that motile cilia defects may contribute to the severity of the phenotype in older *Bbs1*$^{M390R/M390R}$ mice. These findings steer the study of hydrocephalus beyond the ciliopathy field as evidenced by the common theme of abnormal cellular signaling in other models of hydrocephalus[14–16,48–51].

We found that NG2$^+$PDGFR-α$^+$ cells have impaired survival and proliferative capacities in BBS, whereas Olig2$^+$ cells, a cell type existing within the same oligodendrocytic lineage, appear normal. This finding suggests that Bbs1 has an essential role in the survival and proliferation of NG2$^+$PDGFR-α$^+$ but not Olig2$^+$ cells. The abnormal survival and proliferative capacities and the reduced populations of NG2$^+$PDGFR-α$^+$ NPCs in the periventricular regions may explain recent observations that patients with BBS and BBS mouse models have reduced white and gray matter volume in the periventricular subcortical structures[19,31,32]. The MRI findings in patients suggest a loss of cerebral tissue as a cause of ventriculomegaly[31,32]. Our data indicate that the underlying cause of reduced cerebral tissue and ventricular dilation in patients with BBS is impaired survival and proliferation of NPCs rather than degeneration of mature neurons and glia.

The impaired PDGFR-α signaling in BBS led us to explore the therapeutic potential of targeting this pathway to modify the hydrocephalic phenotype early in development. We targeted two downstream effector proteins in the PDGFR-α signaling cascade, AKT and GSK3-β, using lithium, a drug that stimulates phosphorylation of these proteins[44–46,52]. Phosphorylation of AKT and GSK3-β has been shown to increase cell survival and proliferation[41–43]. We found that lithium treatment selectively rescues NG2$^+$PDGFR-α$^+$ cell proliferation by stimulating the phosphorylation of GSK3-β, leading to a reduction in the size of the dilated ventricles in *Bbs1* mutant mice. These results are consistent with those of previous studies demonstrating that lithium stimulates NPC proliferation by increasing the phosphorylation of GSK3-β, thereby suppressing its activity[44–46,52]. Although lithium rescues cell proliferation, it has no statistically significant effect on the cell death of NG2$^+$PDGFR-α$^+$ NPCs. This finding may explain the partial rescue of the hydrocephalic phenotype. Rescue of both cell proliferation and apoptosis may result in a further reduction in ventricular size. To our knowledge, we are the first to target NPC development as a therapy to treat hydrocephalus in any model organism.

In addition, our results demonstrate that BBS proteins have a crucial role in PDGFR-α signaling and NG2$^+$PDGFR-α$^+$ NPC development in the central nervous system. The trafficking function of the BBSome is disrupted in BBS mutant mice[30]. As a result, signaling proteins are mislocalized, leading to an abnormal cellular response[23,30,53,54]. Our findings suggest that the aberrant PDGFR-α signaling in *Bbs1*$^{M390R/M390R}$ mice originates from the mistrafficking of PDGFR-α on the basis of our observations that PDGFR-α interacts with primary components of the BBSome and, hence, is a new cargo protein of the BBSome. However, the exact mechanism underlying the PDGFR-α signaling defects in BBS remains to be elucidated.

By targeting GSK3-β, we rescued the development of NG2$^+$PDGFR-α$^+$ NPCs and hydrocephalus in *Bbs1*$^{M390R/M390R}$ mice. The strategy of targeting downstream effectors of signaling defects may be applicable to other BBS-associated phenotypes.

METHODS

Methods and any associated references are available in the online version of the paper.

Note: Supplementary information is available in the online version of the paper.

ACKNOWLEDGMENTS

We thank L. Biesecker for help obtaining the human MRI scans. We thank K. Rahmouni and D.-F. Guo for help with quantitative RT-PCR and infusion experiments. We thank K. Agassandian for help with dye injection and CSF collection. We thank V. Buffard and L. Qian for their excellent technical assistance. We also appreciate valuable assistance from the University of Iowa Central Microscopy Research Facility. This work was supported in part by US National Institutes of Health grants R01EY110298 and R01EY017168 (to V.C.S.), R01EY022616 (to S.S.), the Knight Templar Eye Foundation (to S.S.) and the Neurosurgery Research and Education Foundation (to T.W.V.). C.S.C. is a National Science Foundation graduate research fellow, and V.C.S. is an Investigator of the Howard Hughes Medical Institute.

AUTHOR CONTRIBUTIONS

C.S.C., T.W.V. and Q.Z. conceived of the project, designed and performed experiments, coordinated collaborations and wrote the manuscript. S.S. contributed to the experimental design and manuscript revisions. R.E.S. and M.D.C. performed transmission electron microscopy, CSF collection and dye injection experiments and revised the manuscript. T.O.M. coordinated microscopic experiments. K.M.K.-N. and P.N. provided and analyzed human MRI scans. D.R.T. performed MRI for all mice. D.Y.N. and C.C.S. designed and developed the *Bbs1* mouse model used in this experiment. K.B. coordinated mouse genotyping and mating. V.C.S. initiated the project, contributed ideas, analyzed and interpreted the results and helped write the manuscript.

COMPETING FINANCIAL INTERESTS

The authors declare no competing financial interests.

Published online at http://www.nature.com/doifinder/10.1038/nm.2996.
Reprints and permissions information is available online at http://www.nature.com/reprints/index.html.

1. Bruni, J.E., Del Bigio, M.R. & Clattenburg, R.E. Ependyma: normal and pathological. A review of the literature. *Brain Res.* **356**, 1–19 (1985).
2. Del Bigio, M.R. Ependymal cells: biology and pathology. *Acta Neuropathol.* **119**, 55–73 (2010).
3. Williams, M.A. *et al.* Priorities for hydrocephalus research: report from a National Institutes of Health–sponsored workshop. *J. Neurosurg.* **107**, 345–357 (2007).
4. Vogel, P. *et al.* Congenital hydrocephalus in genetically engineered mice. *Vet. Pathol.* **49**, 166–181 (2012).
5. Simon, T.D. *et al.* Hospital care for children with hydrocephalus in the United States: utilization, charges, comorbidities, and deaths. *J. Neurosurg. Pediatr.* **1**, 131–137 (2008).
6. Shannon, C.N. *et al.* The economic impact of ventriculoperitoneal shunt failure. *Journal J. Neurosurg. Pediatr.* **8**, 593–599 (2011).
7. Van Camp, G. *et al.* A duplication in the L1CAM gene associated with X-linked hydrocephalus. *Nat. Genet.* **4**, 421–425 (1993).
8. Chi, J.H., Fullerton, H.J. & Gupta, N. Time trends and demographics of deaths from congenital hydrocephalus in children in the United States: National Center for Health Statistics data, 1979 to 1998. *J. Neurosurg.* **103**, 113–118 (2005).
9. Zhang, J., Williams, M.A. & Rigamonti, D. Genetics of human hydrocephalus. *J. Neurol.* **253**, 1255–1266 (2006).

10. Banizs, B. *et al.* Dysfunctional cilia lead to altered ependyma and choroid plexus function, and result in the formation of hydrocephalus. *Development* **132**, 5329–5339 (2005).
11. Patwardhan, R.V. & Nanda, A. Implanted ventricular shunts in the United States: the billion-dollar-a-year cost of hydrocephalus treatment. *Neurosurgery* **56**, 139–144 (2005).
12. Vogel, T.W., Carter, C.S., Abode-Iyamah, K., Zhang, Q. & Robinson, S. The role of primary cilia in the pathophysiology of neural tube defects. *Neurosurg. Focus* **33**, E2 (2012).
13. Spassky, N. *et al.* Adult ependymal cells are postmitotic and are derived from radial glial cells during embryogenesis. *J. Neurosci.* **25**, 10–18 (2005).
14. Tissir, F. *et al.* Lack of cadherins Celsr2 and Celsr3 impairs ependymal ciliogenesis, leading to fatal hydrocephalus. *Nat. Neurosci.* **13**, 700–707 (2010).
15. Talos, F. *et al.* p73 is an essential regulator of neural stem cell maintenance in embryonal and adult CNS neurogenesis. *Cell Death Differ.* **17**, 1816–1829 (2010).
16. Yang, A. *et al.* p73-deficient mice have neurological, pheromonal and inflammatory defects but lack spontaneous tumours. *Nature* **404**, 99–103 (2000).
17. Drake, J.M. The surgical management of pediatric hydrocephalus. *Neurosurgery* **62** (suppl. 2), 633–640 (2008).
18. Drake, J.M., Kestle, J.R. & Tuli, S. CSF shunts 50 years on—past, present and future. *Childs Nerv. Syst.* **16**, 800–804 (2000).
19. Davis, R.E. *et al.* A knockin mouse model of the Bardet-Biedl syndrome 1 M390R mutation has cilia defects, ventriculomegaly, retinopathy, and obesity. *Proc. Natl. Acad. Sci. USA* **104**, 19422–19427 (2007).
20. Ibañez-Tallon, I. *et al.* Dysfunction of axonemal dynein heavy chain Mdnah5 inhibits ependymal flow and reveals a novel mechanism for hydrocephalus formation. *Hum. Mol. Genet.* **13**, 2133–2141 (2004).
21. Lancaster, M.A., Schroth, J. & Gleeson, J.G. Subcellular spatial regulation of canonical Wnt signalling at the primary cilium. *Nat. Cell Biol.* **13**, 700–707 (2011).
22. Ocbina, P.J., Eggenschwiler, J.T., Moskowitz, I. & Anderson, K.V. Complex interactions between genes controlling trafficking in primary cilia. *Nat. Genet.* **43**, 547–553 (2011).
23. Zhang, Q., Seo, S., Bugge, K., Stone, E.M. & Sheffield, V.C. BBS proteins interact genetically with the IFT pathway to influence SHH-related phenotypes. *Hum. Mol. Genet.* **21**, 1945–1953 (2012).
24. Schneider, L. *et al.* PDGFRαα signaling is regulated through the primary cilium in fibroblasts. *Curr. Biol.* **15**, 1861–1866 (2005).
25. Kriegstein, A. & Alvarez-Buylla, A. The glial nature of embryonic and adult neural stem cells. *Annu. Rev. Neurosci.* **32**, 149–184 (2009).
26. Han, Y.G. *et al.* Hedgehog signaling and primary cilia are required for the formation of adult neural stem cells. *Nat. Neurosci.* **11**, 277–284 (2008).
27. Breunig, J.J. *et al.* Primary cilia regulate hippocampal neurogenesis by mediating sonic hedgehog signaling. *Proc. Natl. Acad. Sci. USA* **105**, 13127–13132 (2008).
28. Sawamoto, K. *et al.* New neurons follow the flow of cerebrospinal fluid in the adult brain. *Science* **311**, 629–632 (2006).
29. Ihrie, R.A. & Alvarez-Buylla, A. Lake-front property: a unique germinal niche by the lateral ventricles of the adult brain. *Neuron* **70**, 674–686 (2011).
30. Nachury, M.V. *et al.* A core complex of BBS proteins cooperates with the GTPase Rab8 to promote ciliary membrane biogenesis. *Cell* **129**, 1201–1213 (2007).
31. Baker, K. *et al.* Neocortical and hippocampal volume loss in a human ciliopathy: a quantitative MRI study in Bardet-Biedl syndrome. *Am. J. Med. Genet. A.* **155A**, 1–8 (2011).
32. Keppler-Noreuil, K.M. *et al.* Brain tissue- and region-specific abnormalities on volumetric MRI scans in 21 patients with Bardet-Biedl syndrome (BBS). *BMC Med. Genet.* **12**, 101 (2011).
33. von Bohlen Und Halbach, O. Immunohistological markers for staging neurogenesis in adult hippocampus. *Cell Tissue Res.* **329**, 409–420 (2007).
34. Raponi, E. *et al.* S100B expression defines a state in which GFAP-expressing cells lose their neural stem cell potential and acquire a more mature developmental stage. *Glia* **55**, 165–177 (2007).
35. Jackson, E.L. *et al.* PDGFR-α$^+$ B cells are neural stem cells in the adult SVZ that form glioma-like growths in response to increased PDGF signaling. *Neuron* **51**, 187–199 (2006).
36. Rivers, L.E. *et al.* PDGFRA/NG2 glia generate myelinating oligodendrocytes and piriform projection neurons in adult mice. *Nat. Neurosci.* **11**, 1392–1401 (2008).
37. Richardson, W.D., Young, K.M., Tripathi, R.B. & McKenzie, I. NG2-glia as multipotent neural stem cells: fact or fantasy? *Neuron* **70**, 661–673 (2011).
38. Tripathi, R.B., Rivers, L.E., Young, K.M., Jamen, F. & Richardson, W.D. NG2 glia generate new oligodendrocytes but few astrocytes in a murine experimental autoimmune encephalomyelitis model of demyelinating disease. *J. Neurosci.* **30**, 16383–16390 (2010).
39. Nishiyama, A., Komitova, M., Suzuki, R. & Zhu, X. Polydendrocytes (NG2 cells): multifunctional cells with lineage plasticity. *Nat. Rev. Neurosci.* **10**, 9–22 (2009).
40. Kondo, T. & Raff, M. Oligodendrocyte precursor cells reprogrammed to become multipotential CNS stem cells. *Science* **289**, 1754–1757 (2000).
41. Datta, S.R. *et al.* Akt phosphorylation of BAD couples survival signals to the cell-intrinsic death machinery. *Cell* **91**, 231–241 (1997).
42. Vivanco, I. & Sawyers, C.L. The phosphatidylinositol 3-Kinase AKT pathway in human cancer. *Nat. Rev. Cancer* **2**, 489–501 (2002).
43. Scheid, M.P. & Woodgett, J.R. PKB/AKT: functional insights from genetic models. *Nat. Rev. Mol. Cell Biol.* **2**, 760–768 (2001).
44. Chalecka-Franaszek, E. & Chuang, D.M. Lithium activates the serine/threonine kinase Akt-1 and suppresses glutamate-induced inhibition of Akt-1 activity in neurons. *Proc. Natl. Acad. Sci. USA* **96**, 8745–8750 (1999).
45. Su, H., Chu, T.H. & Wu, W. Lithium enhances proliferation and neuronal differentiation of neural progenitor cells *in vitro* and after transplantation into the adult rat spinal cord. *Exp. Neurol.* **206**, 296–307 (2007).
46. Li, H. *et al.* Lithium-mediated long-term neuroprotection in neonatal rat hypoxia-ischemia is associated with antiinflammatory effects and enhanced proliferation and survival of neural stem/progenitor cells. *J. Cereb. Blood Flow Metab.* **31**, 2106–2115 (2011).
47. Lechtreck, K.F., Delmotte, P., Robinson, M.L., Sanderson, M.J. & Witman, G.B. Mutations in Hydin impair ciliary motility in mice. *J. Cell Biol.* **180**, 633–643 (2008).
48. Goto, J., Tezuka, T., Nakazawa, T., Sagara, H. & Yamamoto, T. Loss of Fyn tyrosine kinase on the C57BL/6 genetic background causes hydrocephalus with defects in oligodendrocyte development. *Mol. Cell. Neurosci.* **38**, 203–212 (2008).
49. Qin, S., Liu, M., Niu, W. & Zhang, C.L. Dysregulation of Kruppel-like factor 4 during brain development leads to hydrocephalus in mice. *Proc. Natl. Acad. Sci. USA* **108**, 21117–21121 (2011).
50. Yung, Y.C. *et al.* Lysophosphatidic acid signaling may initiate fetal hydrocephalus. *Sci. Transl. Med.* **3**, 99ra87 (2011).
51. Rivière, J.B. *et al. De novo* germline and postzygotic mutations in *AKT3*, *PIK3R2* and *PIK3CA* cause a spectrum of related megalencephaly syndromes. *Nat. Genet.* **44**, 934–940 (2012).
52. Azim, K. & Butt, A.M. GSK3β negatively regulates oligodendrocyte differentiation and myelination *in vivo*. *Glia* **59**, 540–553 (2011).
53. Berbari, N.F., Lewis, J.S., Bishop, G.A., Askwith, C.C. & Mykytyn, K. Bardet-Biedl syndrome proteins are required for the localization of G protein–coupled receptors to primary cilia. *Proc. Natl. Acad. Sci. USA* **105**, 4242–4246 (2008).
54. Seo, S. *et al.* Requirement of Bardet-Biedl syndrome proteins for leptin receptor signaling. *Hum. Mol. Genet.* **18**, 1323–1331 (2009).

ONLINE METHODS

Animals. We used male and female mice on a pure 129/SvEv genetic background for *Bbs1*$^{M390R/M390R}$ mice and littermate controls. We generated PDGFR-α^{Cre} (control) and *Bbs1*^{CKO} mice by crossing *Bbs1*$^{loxP/loxP}$ mice (129/SvEv) with PDGFR-α^{Cre} mice (C57BL/6NJ) (Jackson Laboratory, Bar Harbor, Maine). We used littermates and age-matched controls for all animal experiments. Animals were generated at the University of Iowa Carver College of Medicine, and all experiments were performed in accordance with the Institute for Animal Care and Use Committee at the University of Iowa (Iowa City, Iowa).

MRI. We obtained human T2-weighted MRI scans from K.M.K.-N. and P.N. at the University of Iowa and L. Biesecker at the Clinical Research Center at the National Institutes of Health in Bethesda, Maryland, USA. Informed consent was obtained for each human subject. Human subject research was approved by the by both the Institutional Review Board of the National Human Genome Research Institute at the National Institutes of Health and the Institutional Review Board of the University of Iowa. For mice, we performed T2-weighted MRI scans while each mouse was under isoflurane-induced anesthesia using a Varian Unity/Inova 4.7 T small-bore MRI system (Varian, Inc., Palo Alto, California) at the University of Iowa. There was an in-plane resolution of 0.13 × 0.25 mm^2 and an approximate slice thickness of 0.6 mm acquired in the axial, sagittal and coronal planes.

Histology, immunohistochemistry, BrdU and TUNEL assays. We sectioned and stained mouse brains fixed by intracardiac perfusion with 4% paraformaldehyde at 7 μm with H&E. All mouse brains derived from fresh frozen tissue were cryosectioned (8-μm sections). For BrdU experiments, we injected mice intraperitoneally with 300 mg per kg body weight BrdU (Sigma, St. Louis, Missouri) and, after 4 h, euthanized them. We double stained cryosections with either an antibody to BrdU (1:200, Abcam, 6326) or a Click-iT TUNEL assay (Life Technologies, Grand Island, New York) according to the manufacturer's protocols and with antibodies to the following: mouse Cre (1:100, Millipore, MAB3120) mouse Nestin (1:200, Abcam, Cambridge, Massachusetts), mouse O4 (1:200, Millipore, MAB345), mouse NeuN (1:200, Millipore, MAB377 and Abcam, 104225), rabbit GFAP (1:500, Abcam, 7260), rabbit NG2 (1:400, Millipore, 5320), rabbit PDGFR-α (1:200, Santa Cruz Biotechnology Inc., Santa Cruz, SC-338, California) and rabbit Olig2 (1:800, Abnova, PAB16940, Walnut, California). We blocked sections with 1% FCS (Life Technologies) plus 0.3% Triton X-100 (Sigma) in PBS for 1 h at 25 °C before incubation with primary antibodies at 4 °C overnight or 25 °C for 1 h. We used Alexa-Fluor goat secondary antibodies (Life Technologies) to image primary antigens and counterstained nuclei with Vectashield containing DAPI (Vector Laboratories, Burlingame, California).

Cell culture. We cultured OLPs from dissociated cortices of P0 mice. We dissociated cortices in trypsin using a P1000 pipette and then added DMEM (Gibco, Grand Island, New York) supplemented with 20% FCS (Gibco) and 1% penicillin-streptomycin (Gibco). We then plated cells in T25 culture flasks (Corning) and cultured them for 7 d, after which cells were shaken overnight in 37 °C at 250 r.p.m. to separate the OLPs. At this point, nearly all of the attached cells were astrocytes, and the unattached cells were OLPs. Next, we removed the media containing the unattached OLPs and plated them on plastic culture dishes (Corning Inc., Corning, New York). We maintained all cells for an additional 2 d or until confluent using DMEM supplemented with 10% FCS and 1% penicillin-streptomycin. Before treatment, all cells were serum starved for 16 h.

PDGF-α treatment of cells and mice. For receptor activation analysis *in vitro*, we treated cells with 50 ng/ml PDGF-α (Cell Signaling Technologies, Danvers, Massachusetts) for 10 min after pretreatment with 8 μM AG1296 (Cayman Chemical Company, Ann Arbor, Michigan) for 30 min. For *in vivo* experiments, we infused PDGF-α (80 ng per day) in vehicle (1 mg/ml BSA in PBS) or vehicle alone into the lateral ventricle of 3-month-old mice for 6 d using a miniosmotic pump per the manufacturer's instructions (Azlet).

Immunoprecipitation and western blotting. We performed *in vitro* immunoprecipitations as previously described[23]. For endogenous immunoprecipitation experiments, we isolated brain cortices from P3 mice, lysed tissues in radioimmunoprecipitation assay buffer containing protease and phosphatase inhibitors (Roche Applied Science, Indianapolis, Indiana) and precleared the lysates with protein G beads (Thermo Fisher Scientific, Rockford, Illinois) overnight at 4 °C. We added a goat antibody to PDGFR-α (1:100, R&D Systems, AF-1062, Minneapolis, Minnesota) and incubated overnight at 4 °C. We next incubated samples with protein G beads for 4 h at 4 °C and then washed them briefly. We performed SDS-PAGE and western blotting as described previously[35] using 10 μg of total protein per lane. We performed western blotting using the SuperSignal West Pico kit (Pierce Biotechnology, Rockford, Illinois) per the manufacturer's instructions. We blocked membranes for 1 h in Tris-buffered saline and Tween 20 plus 5% milk or BSA and then incubated them overnight at 4 °C with primary antibodies to the following: mouse Flag[30], mouse GFP[30], rabbit BBS2 (ref. 30), rabbit BBS4 (ref. 30), rabbit BBS8 (ref. 30), rabbit BBS9 (ref. 30), rabbit pPDGFR-α (Tyr720) (1:1,000, Sigma, P8246) and goat PDGFR-α (1:5,000, R&D Systems, AF-1062), as well as antibodies to the following from Cell Signaling Technologies: rabbit pAKT (Ser473) (1:5,000, 4060), mouse pAKT (1:1,000, 4051), rabbit AKT (1:1,000, 4691), rabbit pGSK3-β (Ser9) (1:1,000, D85E12) and rabbit GSK3-β (1:1,000, 27C10).

Quantitative RT-PCR experiments. We euthanized mice by CO_2 asphyxiation and excised four brain regions, including the cortex, hypothalamus, hippocampus and cerebellum. We extracted mRNA using TRIzol reagent (Life Technologies). We performed real-time RT-PCR to compare the mRNA levels of BBS1 between the control and BBS1 conditional knockout tissues. We used the following BBS1 primers: 5′-TTCTGCAGCTGGAGCTGAGTG-3′ (forward) and 5′-TCAGTGCCTAGCACCAGACAG-3′ (reverse). RPL19 was used as an internal control.

Lithium therapy. We treated mice with lithium chloride (Sigma) in drinking water using a dose of 1.2 g/l starting from E14.5 (through pregnant and nursing dams). The drug was dissolved in double-distilled water.

Electron microscopy. We obtained scanning electron micrographs of the lateral wall of the lateral ventricles dissected from mice using a Hitachi S-4800 scanning electron microscope (Hitachi, Pleasanton, California). We also obtained transmission electron micrographs of choroid plexi using a Gatan UltraScan 1000 (Pleasonton, California) 2kx2k charge-coupled device digital camera.

Dye injection and visualization of CSF flow. We anesthetized adult mice and injected Evans blue dye into the lateral ventricles. The syringe was left in for 20 min to prevent CSF loss and allow the CSF to circulate. We then euthanized and cryopreserved mice at −20 °C. The next day, the frozen heads were cut in the sagittal plane and imaged.

CSF collection and analysis. We anesthetized adult mice and inserted a glass micropipette into the cisterna magna for CSF collection. We froze all collected samples at −20 °C until analysis. We measured the chloride and sodium ion content using ion-specific electrodes (Roche/Hitachi, Indianapolis, Indiana) in the Pathology Laboratory of the University of Iowa Hospitals and Clinics.

Image analysis and statistics. We cropped all images and adjusted the brightness and contrast using Adobe Photoshop CS5. For immunofluorescent images, we adjusted the brightness and contrast using Zen Light. We performed all cell quantifications, cross-sectional area analyses and volumetric analyses using ImageJ (NIH). We performed statistical comparisons using unpaired *t* tests. Mean values ± s.e.m. are reported.